The Astrophysical Journal, 724:887–894, 2010 December 1 doi:10.1088/0004-637X/724/2/887

THE ROLE OF METHANOL IN THE CRYSTALLIZATION OF TITAN'S PRIMORDIAL OCEAN

Frédéric Deschamps[1], Olivier Mousis[2], Carmen Sanchez-Valle[3], and Jonathan I. Lunine[4]
[1] Institute of Geophysics, Swiss Federal Institute of Technology Zurich, 8092 Zurich, Switzerland; frederic.deschamps@erdw.ethz.ch
[2] Université de Franche-Comté, Institut UTINAM, CNRS/INSU, UMR 6213, 25030 Besançon Cedex, France
[3] Institute of Geochemistry and Petrology, Swiss Federal Institute of Technology Zurich, 8092 Zurich, Switzerland
[4] Dipartimento di Fisica, Università degli Studi di Roma "Tor Vergata," Rome, Italy
Received 2010 May 25; accepted 2010 September 20; published 2010 November 9

ABSTRACT

A key parameter that controls the crystallization of primordial oceans in large icy moons is the presence of anti-freeze compounds, which may have maintained primordial oceans over the age of the solar system. Here we investigate the influence of methanol, a possible anti-freeze candidate, on the crystallization of Titan's primordial ocean. Using a thermodynamic model of the solar nebula and assuming a plausible composition of its initial gas phase, we first calculate the condensation sequence of ices in Saturn's feeding zone, and show that in Titan's building blocks methanol can have a mass fraction of ∼4 wt% relative to water, i.e., methanol can be up to four times more abundant than ammonia. We then combine available data on the phase diagram of the water–methanol system and scaling laws derived from thermal convection to estimate the influence of methanol on the dynamics of the outer ice I shell and on the heat transfer through this layer. For a fraction of methanol consistent with the building blocks composition we determined, the vigor of convection in the ice I shell is strongly reduced. The effect of 5 wt% methanol is equivalent to that of 3 wt% ammonia. Thus, if methanol is present in the primordial ocean of Titan, the crystallization may stop, and a sub-surface ocean may be maintained between the ice I and high-pressure ice layers. A preliminary estimate indicates that the presence of 4 wt% methanol and 1 wt% ammonia may result in an ocean of thickness at least 90 km.

Key words: convection – planets and satellites: composition – planets and satellites: formation – planets and satellites: individual (Titan) – planets and satellites: interiors – planets and satellites: physical evolution

Online-only material: color figures

1. INTRODUCTION

The presence of a sub-surface ocean in the interior of large icy moons was first proposed by Lewis (1971) as a consequence of the phase diagram of water, in which the Clapeyron slope changes from negative to positive at a pressure of 0.21 GPa. As it cools down, the primordial ocean crystallizes both at its top and at its bottom, and if the heat transfer in the outer ice I layer is not efficient enough, a liquid ocean can be maintained in between the low- and high-pressure ice shells. Since Lewis (1971), sub-surface oceans were proposed to exist in most of the large icy moons, including Titan (e.g., Sohl et al. 2003; Grasset et al. 2000; Spohn & Schubert 2003). Their presence is consistent with numerical modeling of thermal convection within the ice I layer (McKinnon 1999; Deschamps & Sotin 2001; Hussmann et al. 2002; Mitri & Showman 2008) and with surface tectonic observations (Carr et al. 1998). However, the most direct hints for their existence come so far from the induced magnetic fields of icy moons, as detected at Ganymede, Callisto, and Europa (Kivelson et al. 1997, 1999, 2000). The shallow origin (a few hundred kilometers deep) of the induced magnetic fields in the Galilean satellites suggests that they are related to electric currents induced in a salty liquid layer beneath the outer ice I layer (Khurana et al. 1998). Evidence for a sub-surface ocean on Titan comes from the analysis of electric field measurements from the *Huygens* probe (Béghin et al. 2009).

The composition of the primordial ocean controls the temperature at the bottom of the outer ice I shell and may play a significant role in the survival of a sub-surface ocean. Because they decrease the temperature at the bottom of outer ice I shell, anti-freeze compounds are of particular importance. The presence of ammonia (NH_3), for instance, strongly reduces the vigor of convection and the efficiency of heat transfer through the ice I layer (Grasset et al. 2000; Deschamps & Sotin 2001; Mitri & Showman 2008).

Another anti-freeze compound that may enter the composition of Titan's primordial ocean is methanol (CH_3OH). Methanol has been observed in a wide range of objects, including star-forming regions (Pilling et al. 2007; Das et al. 2008) and solar system bodies. In particular, methanol has been observed by spectroscopy in several comets (Bockelée-Morvan et al. 2004; Remijan et al. 2008). Moreover, methanol has been tentatively detected on the surface of Enceladus (Hodyss et al. 2009), and Cassini Ion and Neutral Mass Spectrometer (INMS) observations show that it exists in the gas plumes of Enceladus, but in smaller quantity than NH_3 (Waite et al. 2009). The presence of methanol has also been invoked on Titan to explain the rheological characteristics of possible cryogenic slurries (Zhong et al. 2009). So far, however, its influence on the crystallization of the primordial ocean has not been investigated.

In the present paper, we first investigate the fraction of methanol relative to water that can be trapped in the building blocks of Saturn's regular satellites. We then use available data on the phase diagram of the water–methanol system to estimate the role of methanol on the crystallization of Titan's primordial ocean and on the dynamics of its outer ice I layer.

2. TRAPPING OF METHANOL IN ICY PLANETESIMALS

Recently measured deuterium to hydrogen ratios in the water grains expelled by the geysers of Enceladus are found to be close to those measured in comets (Waite et al. 2009). Thanks to this observation, it is now established that the building blocks of Titan were initially formed in the solar nebula instead of

Saturn's subnebula (Mousis et al. 2009a, 2009b, 2009c). We then focus our attention on the formation sequence of the different ices produced in Saturn's formation zone in the solar nebula. Indeed, once formed, these ices will add to the composition of the planetesimals accreted by Saturn itself and its surrounding satellite system.

In our model, the composition of the initial gas phase of the disk is defined as follows: we assume that the abundances of all elements, including oxygen, are protosolar (Lodders 2003) and that O, C, and N exist only in the form of H_2O, CO, CO_2, CH_3OH, CH_4, N_2, and NH_3. The abundances of CO, CO_2, CH_3OH, CH_4, N_2, and NH_3 are then determined from the adopted $CO/CO_2/CH_3OH/CH_4$ and N_2/NH_3 gas phase molecular ratios. Once the abundances of these molecules are fixed, the remaining O gives the abundance of H_2O. Concerning the distribution of elements in the main volatile molecules, we set $CO/CO_2/CH_3OH/CH_4 = 70/10/2/1$ in the gas phase of the disk, values that are consistent with the ISM measurements considering the contributions of both gas and solid phases in the lines of sight (Frerking et al. 1982; Ohishi et al. 1992; Ehrenfreund & Schutte 2000; Gibb et al. 2000). In addition, S is assumed to exist in the form of H_2S, with $H_2S/H_2 = 0.5 \times (S/H_2)_\odot$, and other refractory sulfide components (Pasek et al. 2005). We also consider $N_2/NH_3 = 10/1$ in the nebula gas phase, a value compatible with thermochemical models of the solar nebula (Lewis & Prinn 1980) and with observations of cometary comae (Hersant et al. 2008). In the following, we adopt these mixing ratios as our nominal model of the solar nebula gas-phase composition.

The process by which volatiles are trapped in icy planetesimals, illustrated in Figure 1, is modeled using the stability curves of stochiometric hydrates, clathrates, and pure condensates, and the thermodynamic path (hereafter called cooling curve) detailing the evolution of temperature and pressure at the current location of Saturn in the solar nebula. We refer the reader to the works of Papaloizou & Terquem (1999) and Alibert et al. (2005) for a full description of the turbulent model of the accretion disk used here. The stability curves of hydrates and clathrates are derived from the Lunine & Stevenson (1985) compilation of published experimental work, in which data are available at relatively low temperatures and pressures. On the other hand, the stability curves of pure condensates used in our calculations are derived from the compilation of laboratory data given in the CRC Handbook of Chemistry and Physics (Lide 2002). The cooling curve intercepts the stability curves of the different ices at particular temperatures and pressures. For each ice considered, the domain of stability is the region located below its corresponding stability curve. The clathration process stops when no more crystalline water ice is available to trap the volatile species. Note that, in the pressure conditions of the solar nebula, CO_2 is the only species that crystallizes at a higher temperature than its associated clathrate. We then assume that solid CO_2 is the only existing condensed form of CO_2 in this environment. Moreover, we have considered only the formation of pure ice of CH_3OH in our calculations since, to our best knowledge, no experimental data concerning the stability curve of its associated clathrate have been reported in the literature. In this study, we assume that the clathration efficiency is total, implying that guest molecules had the time to diffuse through porous water–ice planetesimals before their accretion by proto-planets or proto-satellites. However, it is important to note that the variation of the clathration efficiency in the disk does not affect the trapping of NH_3 and CH_3OH in planetesimals because these two species do not form clathrates in the nebula. In the present case, NH_3, H_2S, Xe, CH_4 and ~40% of CO form NH_3–H_2O hydrate and H_2S, Xe, CH_4, and CO clathrates with the available water in the outer nebula. The remaining CO, as well as N_2, Kr, and Ar, whose clathration normally occurs at lower temperatures, remain in the gas phase until the nebula cools enough to allow the formation of pure condensates.

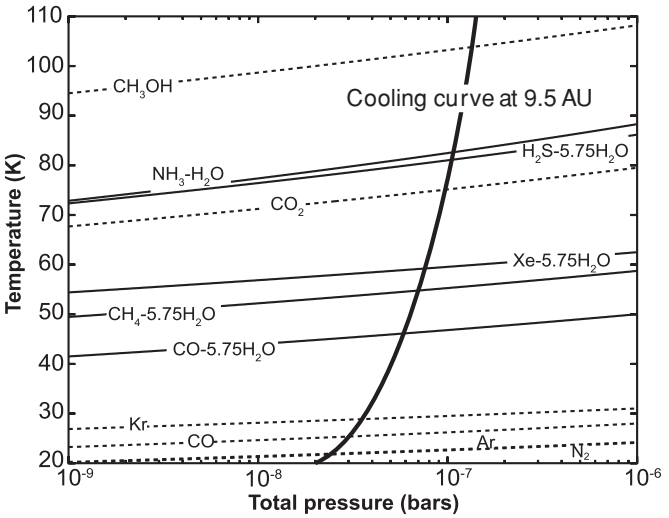

Figure 1. Equilibrium curves of NH_3–H_2O hydrate, H_2S, Xe, CH_4, and CO clathrates (solid lines), CH_3OH, and CO_2 pure condensates (dotted lines), and thermodynamic path followed by the Solar nebula at 9.5 AU as a function of time, respectively, assuming a full efficiency of clathration. Abundances of various elements are solar, with $CO/CO_2/CH_3OH/CH_4 = 70/10/2/1$, $H_2S/H_2 = 0.5 \times (S/H_2)_\odot$, and $N_2/NH_3 = 10/1$ in the gas phase of the disk. Species remain in the gas phase above the stability curves. Below, they are trapped as clathrates or simply condense.

Knowing the thermodynamic conditions occurring during the trapping or condensation of the different volatiles, it is possible to determine the volatile, i, to water mass ratio in planetesimals accreted from the different ices via the following relation (Mousis & Gautier 2004):

$$m_i = \frac{X_i}{X_{H_2O}} \frac{\Sigma(r; T_i, P_i)}{\Sigma(r; T_{H_2O}, P_{H_2O})}, \quad (1)$$

where X_i and X_{H_2O} are the mass mixing ratios of the volatile i and H_2O with respect to H_2 in the nebula, respectively. $\Sigma(r; T_i, P_i)$ and $\Sigma(r; T_{H_2O}, P_{H_2O})$ are the surface density of the nebula at a distance r from the Sun at the epoch of condensation or hydration of the species i (with $i = CH_3OH$ or NH_3), and at the epoch of condensation of water, respectively. Our model allows us to infer that m_{CH_3OH} and m_{NH_3} are about 4 wt% and 1 wt% in icy planetesimals formed at ~9.5 AU in the solar nebula. This implies that, for the adopted gas-phase conditions in the primordial nebula, which can be considered as "standard" conditions, Saturn's regular icy satellites were formed from building blocks containing four times more CH_3OH than NH_3 in mass.

The CH_3OH/NH_3 mass ratio derived from our calculations is at least one order of magnitude larger than the one determined in the plume of Enceladus (Waite et al. 2009). This latter measurement, however, may not reflect the primitive composition of the body. Indeed, the internal environment of Enceladus is inferred to be or have been favorable for aqueous, catalytic chemistry, implying the synthesis of many complex compounds that can be found in the plumes (Matson et al. 2007). In contrast, our

calculation is found to be consistent with the CH_3OH/NH_3 mass ratios ranging between ~2 and 8 in comets 1P/Halley, C/1995 O1 Hale–Bopp, and C/1996 B2 Hyakutake (Bockelée-Morvan et al. 2004). However, even if comets are presumed to be more primitive than a large and evolved body such as Enceladus, their current composition might not reflect that of the planetesimals from which they accreted since they have experienced some collisional activity, leading to a possible alteration of their structure and composition (Marboeuf et al. 2009). It is thus difficult to compare the fraction of methanol predicted in planetesimals by our model to those observed in bodies of the current solar system.

3. CRYSTALLIZATION AND DYNAMICS OF THE ICE I SHELL: INFLUENCE OF METHANOL

3.1. The Phase Diagram of the H_2O–CH_3OH System

Like ammonia, methanol is a powerful anti-freeze. At zero pressure, pure methanol freezes at 175 K, and the temperature of crystallization rises to 205 K and 248 K at 0.25 GPa and 1 GPa, respectively (Figure 2(b); Würflinger & Landau 1977; Gromnitskaya et al. 2004). The phase diagram of the H_2O–CH_3OH system at ambient pressure is well known (Figure 2(a); Vuillard & Sanchez 1961; Miller & Carpenter 1964; Kargel 1992) and indicates that the temperature of crystallization reaches a minimum value of 150 K at the eutectic composition, which is obtained for a weight fraction of CH_3OH of 0.88. Still at ambient pressure, the temperature of crystallization of a solution containing 10% of CH_3OH is lower than that of pure H_2O by 10 K. At higher pressure, there is so far no constraint on the phase diagram of the H_2O–CH_3OH system. First-order estimates can however be deduced from a two-dimensional interpolation of the phase diagrams plotted in Figure 2. In the present study, we determined the crystallization temperature at pressure P and weight fraction of methanol x_{CH_3OH}, first by interpolating the melting temperature at ambient pressure from Figure 2(a), and then by scaling this temperature according to the difference between the melting temperatures for pure water and pure methanol at pressure P (Figure 2(b)).

3.2. Dynamics of the Outer Ice I Shell

Convection is the most efficient and therefore the dominant process of heat and mass transfer through the outer shells of many icy satellites (e.g., Grasset et al. 2000; Deschamps & Sotin 2001; McKinnon 2006). Because the viscosity of ice I is strongly temperature dependent (e.g., Goodman et al. 1981; Durham et al. 1997; Goldsby & Kohlstedt 1997), it is reasonable to assume that thermal convection in the outer ice layer follows the stagnant lid regime. In this regime, a rigid, stagnant lid develops at the top of the fluid, and convection is confined in a sub-layer (e.g., Davaille & Jaupart 1993; Moresi & Solomatov 1995; Deschamps & Sotin 2000). Heat is transported by conduction throughout the stagnant lid, and as a consequence the overall heat transfer through the ice I layer is reduced. With increasing thermal viscosity contrast the thickness of the stagnant lid increases, and the efficiency of the convective heat transfer relative to the conductive heat transfer, measured by the Nusselt number Nu, decreases. The Nusselt number thus depends on both the Rayleigh number Ra, which controls the vigor of convection, and the thermal viscosity contrast (e.g., Moresi & Solomatov 1995; Deschamps & Sotin 2000). The temperature jump across the bottom thermal boundary layer, and thus the temperature of the well mixed interior, is controlled by the thermal viscosity

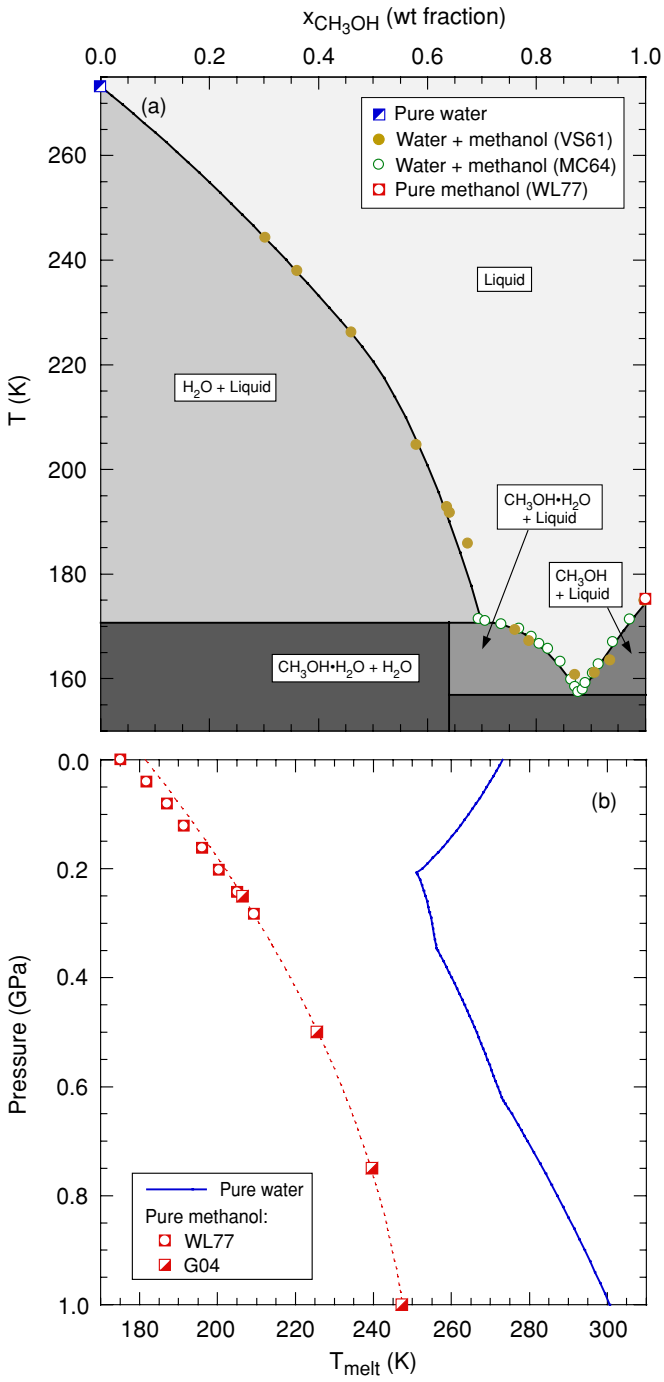

Figure 2. (a) Phase diagram of the H_2O–CH_3OH system at ambient pressure (modified from Kargel 1992). The brown points and green circles are from Vuillard & Sanchez (1961) and Miller & Carpenter (1964), respectively. (b) Phase diagram of pure water (blue curve) and pure methanol (red symbols) up to 1 GPa. The phase diagram of water is from Chizov (1993), and that of methanol from Würflinger & Landau (1977) and Gromnitskaya et al. (2004). The red dotted curve is interpolated from the data of Gromnitskaya et al. (2004).

(A color version of this figure is available in the online journal.)

contrast (Davaille & Jaupart 1993; Deschamps & Sotin 2000). Because the curvature of the outer ice I layer is small, scaling laws obtained in the Cartesian geometry are appropriate to describe convection within it. In this study, we have used scaling laws proposed by Deschamps & Sotin (2000). The temperature of the well-mixed convective sub-layer, T_m, and the average

surface heat flux, $\Phi_{\rm surf}$, are given by

$$T_m = T_{\rm bot} - \Delta T\left(\frac{1.43}{\gamma} - 0.03\right), \quad (2)$$

and

$$\Phi_{\rm surf} = \Phi_{\rm cond} Nu = 3.8\Phi_{\rm cond}\frac{Ra_m^{0.258}}{\gamma^{1.63}}, \quad (3)$$

where

$$\Phi_{\rm cond} = k_I \Delta T/b \quad (4)$$

is the conductive heat flux,

$$\gamma = \frac{\Delta T}{\mu(T_m)}\frac{d\mu}{dT}\Big|_{T=T_m} \quad (5)$$

is the logarithmic thermal viscosity contrast, $\mu(T)$ is the viscosity of ice I at temperature T, T_m is the temperature of the well-mixed convective sub-layer, $T_{\rm bot}$ is the temperature at the bottom of the ice I layer, ΔT is the super-adiabatic temperature difference across the ice I layer, k_I is the thermal conductivity of the ice I, b is the thickness of the ice I layer, and Ra_m is the bulk Rayleigh number (i.e., calculated with the viscosity at temperature T_m, $\mu_m = \mu(T_m)$). With the properties of ice I, the bulk Rayleigh number of an ice I shell of thickness b is

$$Ra_m = \frac{\alpha_I \rho_I g \Delta T b^3}{\mu_m \kappa_I}, \quad (6)$$

where g is the acceleration of gravity, α_I is the thermal expansion, and κ_I is the thermal diffusivity.

The Rayleigh number controls the vigor of convection within the ice I layer. If it is smaller than a critical value that, in the case of the stagnant lid regime, depends on the thermal viscosity contrast (Stengel et al. 1982), the ice I layer is stable and transports heat by conduction. With the viscosity law and rheological properties of ice I discussed in Sections 3.3 and 3.4, the critical Rayleigh number is around 1.4×10^6. Because in our case the thermal viscosity contrast depends on the bulk temperature (Section 3.3), which in turn depends on the temperature at the bottom of the ice I layer, the critical Rayleigh number varies slightly (by about 5%, at most), depending on the composition of the ocean. The Rayleigh number of the ice I layer (Equation (6)) depends on the cube of the layer's thickness, i.e., the ice I layer convects only if it is thick enough. Thus, as the primordial ocean crystallizes, the ice I layer first undergoes a stage in which it is stable with respect to convection and transports heat by conduction. The surface heat flux controls the amount of heat that can be extracted from the satellite's interior. Sources of heat include the cooling of the core and the latent heat of crystallization of the ice I and high-pressure ice (III, V, and VI) layers. Another source of heat that we neglected here, but may have a significant contribution, is the tidal dissipation. If the heat flux generated by these sources is larger than the convective heat flux, the ocean is heating up, and crystallization stops.

3.3. Outline of the Calculations

To estimate the influence of methanol on the dynamics of the outer ice I layer of Titan, we have calculated its Rayleigh number and the heat flux through it as a function of its thickness for initial weight fraction of methanol between 1% and 20%. Note that because methanol remains in the ocean until the eutectic composition is reached, the weight fraction of methanol in the ocean ($x_{\rm CH_3OH}$) increases with increasing thickness of the ice I shell. Details of the calculations can be found in Deschamps & Sotin (2001). First, we calculate the temperature at the bottom of the ice I layer ($T_{\rm bot}$) as a function of the ice I layer thickness b and of the initial weight fraction of methanol in the ocean using an iterative Newton–Raphson method. The thickness (b) gives access to the pressure at the bottom of the ice I layer. By definition, the temperature at the bottom of the ice I layer is equal to the crystallization temperature at this depth, which we interpolate from the phase diagrams in Figure 2. Assuming that the ocean is adiabatic, we then calculate the thickness of the ocean from the depth of the liquid/high pressure ice transition, and update $x_{\rm CH_3OH}$ and $T_{\rm bot}$. The initial thickness of the ocean is prescribed as an input parameter. Second, we calculate the temperature of the well-mixed interior T_m from the scaling law (2). We assume that the viscosity of ice I follows the relationship

$$\mu(T) = \mu_{\rm ref}\exp\left[\frac{E_a}{RT_{\rm ref}}\left(\frac{T_{\rm ref}}{T} - 1\right)\right], \quad (7)$$

where E_a is the activation energy of ice I, R is the ideal gas constant, and $\mu_{\rm ref}$ is the reference viscosity at temperature $T_{\rm ref}$. With this definition of the viscosity, the logarithmic thermal viscosity contrast is given by

$$\gamma = \frac{E_a \Delta T}{RT_m^2}. \quad (8)$$

Replacing γ by this expression in Equation (2), T_m is the solution of a degree 2 polynomial. With the calculated value of T_m, and using the properties of ice I listed in Table 1, we then calculate the viscosity (Equation (7)), the bulk Rayleigh number (Equation (6)), and the heat flux through the ice I shell (Equation (3)). Furthermore, we have calculated the thickness of the thermal lithosphere, defined by the thickness of ice I through which heat is transferred by conduction.

$$b_{\rm th} = \frac{k_I(T_m - T_{\rm surf})}{\phi_{\rm surf}}. \quad (9)$$

The thickness of the thermal lithosphere gives a rough estimate of the mechanical lithosphere, and thus of the lithospheric strength.

Table 1
Physical, Thermodynamical, and Rheological Properties

Properties	Symbol	Value
Physical properties of Titan		
Radius (km)	R	2575
Radius of the silicate layer	R_S	1800
Density (kg m^{-3})	ρ	1881
Acceleration of gravity (m s^{-3})	g	1.35
Surface temperature (K)	$T_{\rm surf}$	94
Properties of ice I		
Density (kg m^{-3})	ρ_I	917
Thermal conductivity (W m^{-1} K^{-1})	k_I	2.6
Thermal expansion (1/K)	α_I	1.56×10^{-4}
Thermal diffusivity (m^3 s^{-1})	κ_I	1.47×10^{-4}
Reference viscosity (Pa s)	$\mu_{\rm ref}$	5.0×10^{13}
Activation energy (kJ mol^{-1})	E_a	60

3.4. Rheology of Ice I

The rheological properties of ice I play a crucial role in the dynamics of the ice I layer. The activation energy E_a of

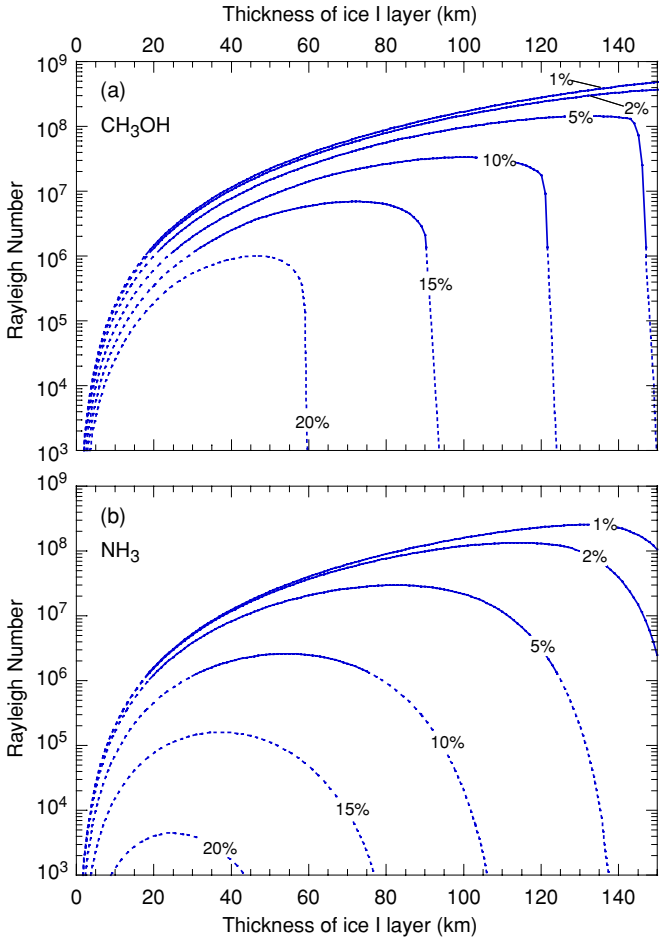

Figure 3. Influence of impurities on the dynamics of the outer ice I shell. Results are plotted as a function of the thickness of the ice I shell. (a) Bulk Rayleigh number for weight fractions of CH_3OH between 1% and 20%. (b) Bulk Rayleigh number for weight fractions of NH_3 between 1% and 20%. The dotted parts of the curves indicate that the Rayleigh number is smaller than the critical Rayleigh number for the onset of convection in the case of a stagnant lid regime, i.e., the ice I layer does not convect.

(A color version of this figure is available in the online journal.)

ice I controls the thermal viscosity contrast through the outer ice I shell, and the Rayleigh number strongly depends on the reference viscosity $\mu_{\rm ref}$. A difficulty is that ice I undergoes different flow regimes depending on the temperature, grain size, and applied stress (e.g., Goodman 1981). The flow regimes relevant to the icy moon interiors are non-Newtonian (stress exponent larger than 1), and include several dislocation creep regimes (depending on the temperature range), superplastic flow, and basal slip (e.g., Durham et al. 1997; Goldsby & Kohlstedt 2001; Durham & Stern 2001). By contrast, the scaling laws for temperature and heat flux (Equations (2) and (3)) we used were built for a Newtonian fluid (stress exponent is equal to one). This problem can be fixed by prescribing lower values of the activation energy, as shown by Dumoulin et al. (1999). The convective heat flux observed for a non-Newtonian fluid with a stress exponent $n = 3$ is similar to that for a Newtonian fluid with an activation energy divided by a factor of 2.

Activation energy can be deduced from flow experiments. The intermediate dislocation creep regime proposed by Durham et al. (1997) is valid in the temperature range 195–240 K, and yields a stress exponent and an activation energy of $n = 4$ and $E_a = 61$ kJ mol^{-1}, respectively. For the superplastic flow regime (and temperatures lower than 255 K), Goldsby & Kohlstedt (2001) found $n = 1.8$ and $E_a = 49$ kJ mol^{-1}, and for the basal slip regime they found $n = 2.4$ and $E_a = 60$ kJ mol^{-1}. Furthermore, the activation energy of the hydrogen and oxygen atomic diffusion in ice I is close to 60 kJ mol^{-1} (Weertman 1983). A reasonable value of the activation energy therefore is in the range of 50–70 kJ mol^{-1}.

The reference viscosity can be estimated from relationships between stress and strain rate, as those measured by Gerrard et al. (1952) for alpine glacier. For a strain rate around 10^{-11} s^{-1}, which is relevant for icy moons, the viscosity of ice I near the melting point is approximately 5.0×10^{13} Pa s. The experiments of Goldsby & Kohlstedt (2001), performed at temperatures well below the melting point, lead to a reference viscosity around 10^{13} Pa s, but for strain rates lower than those considered by Goldsby & Kohlstedt (2001), the reference viscosity is larger, around 10^{14} Pa s. It is thus reasonable to define the reference viscosity as the viscosity close to the melting point (i.e., for $T_{\rm ref}$ equal to the melting temperature of pure water), and to set its value to 5.0×10^{13} Pa s.

4. RESULTS

We applied the method described above to the case of Titan, using the properties listed in Table 1. We assumed a radius of the silicate layer of 1800 km, i.e., the initial thickness of the ocean is equal to 775 km. Results are shown in Figures 3 and 4. To account for the uncertainties in the flow regime and activation energy, and for the fact that our scaling laws were built for a Newtonian fluid, we performed additional calculations varying the activation energy between 30 and 90 kJ mol^{-1}, but found that its influence is small compared to that of the weight fraction of methanol. The reference viscosity is more sensitive, and increasing $\mu_{\rm ref}$ by one order of magnitude decreases the Rayleigh number by one order of magnitude and the surface heat flux by about a factor of 2.

Figure 3(a) plots the bulk Rayleigh number Ra_m for initial weight fraction of methanol $x^{\rm init}_{\rm CH_3OH}$ in the ocean between 1% and 20%. For comparison, Figure 3(b) shows similar calculations for an initial weight fraction of ammonia (NH_3) in the range 1%–20%. The dashed parts of the curves indicate that the ice I layer does not convect (Ra_m is lower than the critical Rayleigh number). Clearly, the presence of methanol in the primordial ocean inhibits convection in the ice I layer. The critical thickness of ice I for the onset of convection in the ice I layer (indicated by the limit between the dashed and plain parts of the curves) increases with increasing $x^{\rm init}_{\rm CH_3OH}$, and for a given thickness of ice I the vigor of convection decreases with increasing $x^{\rm init}_{\rm CH_3OH}$. Because the temperature at the bottom of the ice I layer decreases with increasing weight fraction of methanol, the bulk viscosity μ_m increases, leading to a drop in the bulk Rayleigh number. More importantly, Ra_m reaches a maximum value and starts to decrease again, i.e., convection in the ice I layer becomes less vigorous. If it is thick enough, the ice I layer is stable again with respect to convection. These effects are similar to that observed for an ocean enriched in ammonia (Grasset & Sotin 1996; Deschamps & Sotin 2001; Mitri & Showman 2008), and results from a competition between the thickness b of the ice I layer and its bulk viscosity μ_m. Because the volume fraction of methanol in the remaining ocean increases as the ice I layer thickens, the bottom temperature $T_{\rm bot}$ decreases more rapidly than in the case of a pure water ocean. The internal temperature T_m sharply decreases, inducing a sharp increase in μ_m. Note that

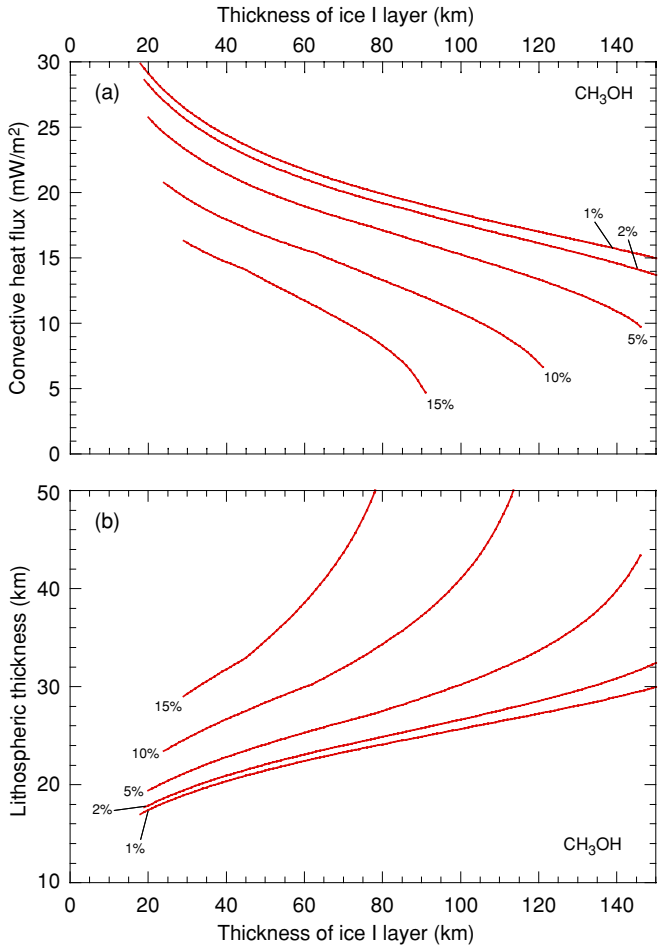

Figure 4. (a) Convective heat flux through the ice I shell (Equation (3)) for weight fractions of CH_3OH between 1% and 20%. (b) Lithospheric thickness (Equation (9)) for weight fractions of CH_3OH between 1% and 20%. Results plotted as a function of the thickness of the ice layer, in the range of thickness for which the ice I layer is unstable.

(A color version of this figure is available in the online journal.)

for $x^{\rm init}_{CH_3OH} = 20\%$, the ice I layer remains stable independent of its thickness. Comparison between Figures 3(a) and (b) indicates that with our current knowledge of the H_2O–CH_3OH phase diagram, the effect of methanol is weaker than that of ammonia. Note that in the case of an ocean enriched in methanol, the decrease in Ra_m is very sharp. This feature is linked to the lack of constraint on the H_2O–CH_3OH phase diagram. At large (>50%) weight fraction of methanol, our interpolation of the temperature of crystallization is no longer accurate.

Assuming an ammonia-rich ocean, Mitri & Showman (2008) noted that, at the convective shut-off, the convective heat flux is larger than the conductive heat flux. They proposed that if the heat flux at the bottom of the ice I layer is between these two values, the mechanism of heat transfer through the ice I layer oscillates between the conductive and stagnant lid convective regimes. Our calculations (for both methanol and ammonia) indicate that the Nusselt number at the convection shut-off is slightly larger than 1 (typically, around 1.1–1.2), i.e., the convective heat flux is about 10%–20% larger than the conductive heat flux. This difference is smaller than that reported by Mitri & Showman (2008), but qualitatively agrees with their hypothesis. Note, however, that within the uncertainties on the Nusselt number scaling law and on the critical Rayleigh number estimate, the Nusselt number at the convection shut-off may be equal to 1.

Figure 4(a) plots the heat flux as a function of the ice I layer for a weight fraction of CH_3OH between 1% and 20% and indicates that the heat transfer through the ice I layer decreases with the increase of both b and $x^{\rm init}_{CH_3OH}$. The Nusselt number is mainly controlled by the Rayleigh number (Equation (3)). The logarithmic thermal viscosity contrast γ increases with decreasing bulk temperature (Equation (8)), but its influence on Nu is of second order compared to that of Ra_m. The evolution of Nu with the thickness of the ice I layer is therefore similar to that of Ra_m, i.e., it increases up to the maximum value, and then decreases as the ice I layer further thickens. The evolution of the convective heat flux with the thickness of the ice I layer results from the combined evolutions of the Rayleigh number (Equation (6)) and the conductive heat flux (Equation (4)). The layer monotonically decreases as the ice I layer thickens. If the ice I layer is not too thick, the Rayleigh number, and thus the Nusselt number, increases. This effect is however overwhelmed by the decrease in conductive heat flux, and on the whole the convective heat flux decreases. If the ice I layer is thick enough, the combined decreases in Rayleigh number and conductive heat flux result in a sharper decrease in the convective heat flux.

Figure 4(b) plots the thickness of the thermal lithosphere (Equation (9)) as a function of the thickness of the ice I layer and for several values of $x^{\rm init}_{CH_3OH}$. The thermal lithosphere thickens with increasing ice I layer. More interestingly, the thermal lithosphere dramatically thickens (i.e., the lithosphere gets stronger), with increasing $x^{\rm init}_{CH_3OH}$. Note that the thermal lithospheric thickness overestimates the mechanical lithospheric thickness. However, this does not change the conclusion that the presence of methanol in the ocean strengthens the lithosphere.

As convection in the ice I layer shuts off, heat is transferred by conduction throughout the ice I shell. The conductive heat flux through this layer (Equation (4)) is small, typically around 2–3 mW m^{-2}, which strongly limits the amount of heat that can be extracted from the ocean toward the surface, and may prevent a complete freezing of the remaining ocean. Our calculations account neither for the possible presence of a conductive layer of clathrates at the top of the ice I layer (Tobie et al. 2006), which induces thermal blanketing at the top of the ice I layer, nor for the production of internal heating by tidal dissipation in the ice I layer, which modifies the convective flow pattern in this layer (see discussion). Because these additional complexities would reduce the amount of heat that can be extracted from the ocean (thus opposing its crystallization), the thickness of the ice I layer at the convection shut-off (as we calculate it) is an upper estimate of the thickness of the outer ice I layer of Titan. A more accurate value of this thickness would also require a detailed calculation of the thermal evolution of Titan. The thickness of ice I layer at the convection shut-off can however be used (together with the outer radius of the high pressures ices, which is calculated in our model) to derive a lower bound of the thickness of the remaining ocean. For an initial weight fraction of methanol of 5%, convection shuts off if the ice I layer is larger than 145 km, and the remaining ocean is 100 km thick. The effects of 5% ammonia are slightly stronger. The thickness of the ice I layer at the convection shut-off and the thickness of the remaining ocean are both equal to 125 km.

Methanol, if present in the primordial ocean of Titan, thus has important consequences on the crystallization of this ocean. A small (around 3%–4% and more) weight fraction of methanol in the primordial ocean would strongly reduce the vigor of

convection of the outer ice I layer and the efficiency of heat transfer through it. If convection cannot accommodate the cooling of the core and the latent heat of crystallization of the ice I and high-pressure ice layers, the crystallization of the ocean stops, and a sub-surface ocean is maintained between the two ice layers.

5. DISCUSSION AND CONCLUSIONS

Our calculations assumed that the main source of heating in icy moons is the radiogenic heating generated in the silicate core (or mantle). However, in the case of satellites that move on sufficiently eccentric orbits, tidal friction may be a significant source of energy throughout the satellite, which would increase the amount of heat available at the bottom of the ice I layer. This has some important consequences on the evolution of icy moons (Tobie et al. 2005, 2006). Furthermore, if tidal dissipation also releases heat within the ice I layer, the convective pattern and the heat transfer through the ice I layer would be strongly affected. Calculations in various geometries (e.g., Travis & Olson 1994; Sotin & Labrosse 1999; Deschamps et al. 2010) showed that an increase in the amount of internal heating reduces the vigor of hot plumes rising from the bottom thermal boundary layer, and the heat transfer through the convective layer is less efficient than in the bottom heating case. Tidal dissipation, if present, may thus play a significant role in the survival of a sub-surface ocean of icy moons. A better description of the influence of tidal heating requires specific scaling laws built from numerical experiments of thermal convection that include a mixed mode of heating.

Future calculations may also include more constraints on the phase diagram of the H_2O–CH_3OH system at pressures up to 1 GPa. The interpolation between the phase diagrams for pure water and pure methanol is valid for weight fraction of methanol up to 40%, but is inaccurate for larger fractions and leads to a wrong description of the outer ice I shell dynamics (Figure 3(a)). Ice physics experiments are thus needed to specify the phase diagram of the H_2O–CH_3OH system for intermediate weight fraction of methanol.

Despite the limitations discussed above, our calculations give qualitative and first order quantitative estimates of the role of methanol in the crystallization of the primordial ocean of Titan. The presence of methanol in this ocean, like that of ammonia, significantly reduces the temperature of crystallization, which in turn reduces the vigor of convection in the outer ice I layer, and the efficiency of heat transfer through it. As a result, the primordial ocean may not complete its crystallization, and a liquid layer may be maintained beneath a 100 to 200 km thick ice I layer. Based on our current knowledge of the phase diagram of the H_2O–CH_3OH system, the calculations we performed indicate that the effect of methanol is slightly less pronounced than that of ammonia. However, because our calculations show that methanol may be more abundant than ammonia in Titan, this compound may have a more pronounced effect than ammonia on the crystallization of the primordial ocean. For instance, the presence of 5% of methanol in weight fraction would have the same effect than the presence of 3% of ammonia (Figure 3).

Based on our model describing the composition of ices formed in the solar nebula (Section 2), the building blocks of Titan may contain up to 1% ammonia and 4% methanol. If the composition for the primordial ocean is similar, we can propose a tentative model for the outer ($R > 1800$ km) radial structure of Titan. It is clear from Figure 1(a) and from previous studies (Grasset et al. 2000; Deschamps & Sotin 2001) that 1% of ammonia alone would have a limited effect on the dynamics of the outer ice I shell of Titan, and on the crystallization of its primordial ocean. Our calculations indicate that convection would shut off for a thickness of ice I of 160 km, i.e., the upper bound for the thickness of the ice I layer and the lower bound for the thickness of the remaining ocean would be 160 and 25 km, respectively. The additional presence of 4% methanol, whose effects are similar to those of ∼2.5% ammonia, is likely to induce significant changes. Assuming that the effects of ammonia and methanol can be linearly added, i.e., the combination of 1% ammonia and 4% methanol is equivalent to 3.5% of ammonia, convection in the outer ice I layer would stop if this layer is thicker than 140 km. Therefore, the thickness of Titan's outer ice I layer would be at most 140 km, and a (at least) 90 km thick ocean would be maintained between this ice I layer and a (at most) 650 km thick shell of high-pressure ice. Again, additional experiments are needed to constrain the phase diagram of the H_2O–NH_3–CH_3OH system, and evaluate more precisely the effect of the combined presence of ammonia and methanol in the primordial oceans of Titan and other icy moons.

Tobie et al. (2006) proposed a scenario for the formation of the methane atmosphere of Titan, in which methane is stored as clathrates in a sub-surface layer after the core overturn, and released afterward during three main outgassing episodes. The last outgassing episode is related to the crystallization of the outer ice I layer and thermal convection within it, and is also likely to occur if the primordial ocean is enriched in methanol instead of ammonia. Two possible origins of Titan's methane are the interaction of the sub-surface liquid water ocean with rocks assumed to constitute the core of the body (Atreya et al. 2006) or its direct capture in the building blocks of the satellite at the time of their formation in the feeding zone of Saturn, this latter hypothesis being the most likely (Mousis et al. 2009a). In both cases, methane migrates toward the top of the primordial ocean during or right after the core overturn (Tobie et al. 2006).

Thus, methanol, if present in the primordial ocean of Titan, may be a key ingredient that controls the crystallization of the liquid phase. Experimental constraints on the phase diagram of the water–methanol system and additional numerical modeling of the dynamics of the ice I layer will quantify more accurately the role of methanol in the evolution of Titan.

We are grateful to an anonymous colleague for his constructive review. This work was partly supported by the Swiss National Science Foundation grant 200021-111870 (F.D.), and by the CNES (O.M.).

REFERENCES

Alibert, Y., Mordasini, C., Benz, W., & Winisdoerffer, C. 2005, A&A, 434, 343
Atreya, S. K., Adams, E. Y., Niemann, H. B., Demick-Montelara, J. E., Owen, T. C., Fulchignoni, M., Ferri, F., & Wilson, E. H. 2006, Planet. Space Sci., 54, 1177
Béghin, et al. 2009, Planet. Space Sci., 57, 1872
Bockelée-Morvan, D., Crovisier, J., Mumma, M. J., & Weaver, H. A. 2004, in Comets II, The Composition of Cometary Volatiles, ed. M. C. Festou, H. U. Keller, & H. A. Weaver (Tucson, AZ: Univ. Arizona Press), 391
Carr, M. H., et al. 1998, Nature, 391, 363
Chizov, V. E. 1993, Prikl. Mekh. Tekh. Fiz., 82, 113
Das, A., Acharyya, K., Chakrabarti, S., & Chakrabarti, S. K. 2008, A&A, 486, 209
Davaille, A., & Jaupart, C. 1993, Geophys. Res. Lett., 20, 1827
Deschamps, F., & Sotin, C. 2000, Geophys. J. Int., 143, 204
Deschamps, F., & Sotin, C. 2001, J. Geophys. Res., 106, 5107
Deschamps, F., Tackley, P., & Nakagawa, T. 2010, Geophys. J. Int., 182, 137
Dumoulin, C., Doin, M.-P., & Fleitout, L. 1999, J. Geophys. Res., 104, 12759

Durham, W. B., Kirby, S. H., & Stern, L. A. 1997, J. Geophys. Res., 102, 16293
Durham, & Stern, L. A. 2001, Ann. Rev. Earth Planet. Sci., 29, 295
Ehrenfreund, P., & Schutte, W. A. 2000, Adv. Space Res., 25, 2177
Frerking, M. A., Langer, W. D., & Wilson, R. W. 1982, ApJ, 262, 590
Gerrard, J. A. F., Perutz, M. F., & Roch, A. 1952, Proc. R. Soc.. A, 207, 554
Gibb, E. L., et al. 2000, ApJ, 536, 347
Goldsby, D. L., & Kohlstedt, D. L. 1997, Proc. 28th Annual Lunar and Planetary Science Conf., 429
Goldsby, D. L., & Kohlstedt, D. L. 2001, J. Geophys. Res., 106, 11017
Goodman, D. J., Frost, H. J. M. F., & Ashby, M. F. 1981, Philos. Mag. A, 43, 665
Grasset, O., & Sotin, C. 1996, Icarus, 123, 101
Grasset, O., Sotin, C., & Deschamps, F. 2000, Planet. Space Sci., 48, 617
Gromnitskaya, E. L., Stal'gorova, O. V., Yagafarov, O. F., Brazhkin, V. V., Lyapin, A. G., & Popova, S. V. 2004, J. Exp. Theor. Phys. Lett., 80, 597
Hersant, F., Gautier, D., Tobie, G., & Lunine, J. I. 2008, Planet. Space Sci., 56, 1103
Hodyss, R., Parkinson, C. D., Johnson, P. V., Stern, J. V., Goguen, J. D., Yung, Y. L., & Kanik, I. 2009, Geophys. Res. Lett., 36, 17103
Hussmann, H., Spohn, T., & Wieczerkowski, K. 2002, Icarus, 156, 143
Kargel, J. S. 1992, Icarus, 100, 556
Khurana, K. K., Kivelson, M. G., Stevenson, D. J., Schubert, G., Russell, C. T., Walker, R. J., & Polanskey, C. 1998, Nature, 395, 777
Kivelson, M. G., Khurana, K. K., Russell, C. T., Volwerk, M., Walker, R. J., & Zimmer, C. 2000, Science, 289, 1340
Kivelson, M. G., et al. 1997, Geophys. Res. Lett., 24, 2155
Kivelson, M. G., et al. 1999, J. Geophys. Res., 104, 4609
Lewis, J. S. 1971, Icarus, 15, 174
Lewis, J. S., & Prinn, R. G. 1980, ApJ, 238, 357
Lide, D. R. 2002, CRC Handbook of Chemistry and Physics : A Ready-reference Book of Chemical and Physical Data, ed. D. R. Lide (83rd ed.; Boca Raton, FL: CRC Press)
Lodders, K. 2003, ApJ, 591, 1220
Lunine, J. I., & Stevenson, D. J. 1985, ApJS, 58, 493
Marboeuf, U., Petit, J.-M., & Mousis, O. 2009, MNRAS, 397, L74
Matson, D. L., Castillo, J. C., Lunine, J., & Johnson, T. V. 2007, Icarus, 187, 569
McKinnon, W. B. 1999, Geophys. Res. Lett., 26, 951
McKinnon, W. B. 2006, Icarus, 183, 435
Miller, G. A., & Carpenter, D. A. 1964, J. Chem. Eng. Data, 9, 371
Mitri, G., & Showman, A. P. 2008, Icarus, 193, 387
Moresi, L.-N., & Solomatov, V. S. 1995, Phys. Fluids, 7, 2154
Mousis, O., & Gautier, D. 2004, Planet. Space Sci., 52, 361
Mousis, O., Lunine, J. I., Pasek, M., Cordier, D., Hunter Waite, J., Mandt, K. E., Lewis, W. S., & Nguyen, M.-J. 2009a, Icarus, 204, 749
Mousis, O., Lunine, J. I., Waite, J. H., Magee, B., Lewis, W. S., Mandt, K. E., Marquer, D., & Cordier, D. 2009b, ApJ, 701, L39
Mousis, O., et al. 2009c, ApJ, 691, 1780
Ohishi, M., Irvine, W. M., & Kaifu, N. 1992, in IAU Symp. 150, Astrochemistry of Cosmic Phenomena, ed. P. D. Singh (Dordrecht: Kluwer), 171
Papaloizou, J. C. B., & Terquem, C. 1999, ApJ, 521, 823
Pasek, M. A., Milsom, J. A., Ciesla, F. J., Lauretta, D. S., Sharp, C. M., & Lunine, J. I. 2005, Icarus, 175, 1
Pilling, S., Neves, R., Santos, A. C. F., & Boechat-Roberty, H. M. 2007, A&A, 464, 393
Remijan, A. J., et al. 2008, ApJ, 689, 613
Sohl, F., Hussmann, H., Schwentker, B., Spohn, T., & Lorenz, R. D. 2003, J. Geophys. Res. (Planets), 108, 5130
Sotin, C., Grasset, O., & Beauchesne, S. 1998, Solar System Ices, Astrophysics and Space Science Library (ASSL) Ser. 227, ed. B. Schmitt, C. de Bergh, & M. Festou (Dordrecht: Kluwer Academic), 79
Sotin, C., & Labrosse, S. 1999, Phys. Earth Planet. Inter., 112, 171
Spohn, T., & Schubert, G. 2003, Icarus, 161, 456
Stengel, K. C., Oliver, D. S., & Booker, J. R. 1982, J. Fluid Mech., 120, 411
Tobie, G., Lunine, J., & Sotin, C. 2006, Nature, 440, 61
Tobie, G., Mocquet, A., & Sotin, C. 2005, Icarus, 177, 534
Travis, B., & Olson, P. 1994, Geophys. J. Int., 118, 1
Vuillard, G., & Sanchez, M. 1961, Bull. Soc. Chim. France, 1961, 1877
Waite, J. H., Jr., et al. 2009, Nature, 460, 487
Weertman, J. 1983, Annu. Rev. Earth Planet. Sci., 11, 215
Würflinger, A., & Landau, R. 1977, J. Phys. Chem. Solids, 38, 811
Zhong, F., Mitchell, K. L., Hays, C. C., Choukroun, M., Barmatz, M., & Kargel, J. S. 2009, Icarus, 202, 607